THE PUBLISHING HOUSE
OF THE ROMANIAN ACADEMY

PROCEEDINGS OF THE ROMANIAN ACADEMY, Series A,
Volume 24, Number 1/2023, pp. 51–60
DOI: 10.59277/PRA-SER.A.24.1.07

WATER EFFECT ON ENERGY EVOLUTION AND FRACTAL CHARACTERISTICS OF COAL SAMPLES UNDER IMPACT LOADING

Zhen WEI[1,3], Ke YANG[2], Litong DOU[1,3], Jiqiang ZHANG[1,3] Shuxin HE[1,3]

[1] Anhui University of Science and Technology, State Key Laboratory of Mining Response and Disaster Prevention and Control in Deep Coal Mines, Huainan, Anhui 232001, China
[2] Hefei Comprehensive National Science Center, Institute of Energy, Hefei 230031, China
[3] Anhui University of Science and Technology, Key Laboratory of Mining Coal Safety and Construction Efficiency of Anhui Province and Ministry of EducationHuainan 232001, China
Corresponding author: Ke YANG, E-mail: keyang2003@163.com

Abstract. The dynamic tensile strength of the coal is critical to the initiation and evolution of dynamic disasters such as coal bump and coal and gas outburst. To investigate mechanical and geometrical characteristics of the coal bump subjected to the variation of the shock pressure and water content, a split Hopkinson pressure bar (SHPB) with ultra-high-speed camera and fractal dimension were employed. The results show that the stress wave is the main controlling factor of a large number of micro damage structures and damage evolution of primary pores and voids in coal samples under impact load, and the coal rock fragmentation is a process of energy absorption and dissipation. With the increase of impact load, the dissipated energy density of coal samples increases linearly, but when the incident energy is small, the dissipated energy density of coal samples has little difference; The fractal dimension of samples increases with the increase of loading pressure, and the increasing rate has a decreasing trend. Under the same loading pressure, the fractal dimension of saturated coal sample is the largest, and that of dry coal sample is the smallest; The deformation and failure of coal samples are mainly tensile splitting, and the failure cracks develop along the loading direction, first in the middle of the disc, and then multiple secondary micro cracks are initiated. It is found that there are several main strain concentration regions in the middle of saturated coal sample under impact load, and the range gradually expands, and finally develops along the radial direction.

***Key words**:* water content, SHPB, energy dissipation, loading rate, fractal dimension.

1. INTRODUCTION

Dynamic disasters represented by gas outburst, mining seismicity and coal bump are critical to the mining safety and production, especially for deep mining [1–2]. The occurrence of the dynamic disaster is closely related to the coal reservoir environment (stress, gas pressure, temperature and seepage condition), and hydromechanical properties (matrix strength, pore-fracture system, water content and component). Based on the field measurement, the higher strength of the surrounding rock is, the more occurrence possibility of the dynamic disasters is, under the disturbance of mining and tunneling activity [3]. Currently, the number of gas outburst related mine exceeds 1000 mines in China. Water-related gas disaster management measures include coal seam infusion by deep-hole, hydraulic fracturing, hydraulic flushing and hydraulic slotting was popularly employed to modify the attribute of the coal, inhibiting the gas outburst and coal bump [4–7]. Behavior of coal, same as that of other soft rocks, is highly dependent water content [8]. Therefore, the percentage of water content significantly affects the mechanical properties of coal and its response to dynamic disturbances. Numerous theoretical and experimental investigations were conducted to study the effect of water content and dynamic disturbances on the coal, and considerable achievement was obtained in recent years.

Combining with the Split Hopkinson Pressure Bar (SHPB), the stress-strain evolution and fracture morphology, fracture toughness, etc. subjected to the variation of internal structure and loading rate and path

were widely studied. Among of them, Deng et al. [9] proposed a new model of energy consumption during rock fragmentation, and the relationship between energy consumption and the rock fragment size distribution was studied. Ai et al. [10] investigated the crack propagation and dynamic mechanical properties of coal under high strain rate loading, finding that bedding directions not only have a major influence on dynamic mechanical properties such as dynamic tensile strength, strain rate and strain energy but also have a great influence on the crack propagation path. Ai et al. [11] established a new calculation method of crack propagation velocity and analyzed the stress-strain characteristics and crack propagation features, combining with the dynamic resistance strain gauge, high-speed camera, and Split Hopkinson Pressure Bar (SHPB). Zhou et al. [12] studied the water saturation effects on dynamic fracture behavior of sandstone, concluding that the different rate dependencies of fracture behaviors between dry and saturated specimens was governed by the combined weakening and enhancing effects of water. Cao et al. [13] investigated the average strain rate (ASR) on the dynamic compressive strength (DCS), microstructure fractal dimensionand failure pattern of the cemented tailings composites (CTC) specimens, based on the Split Hopkinson Pressure Bar (SHPB) and scanning electron microscopy (SEM) system. Zhou et al. [14] investigated the deterioration of dynamic fracture characteristics, tensile strength and elastic modulus of tight sandstone under dry-wet cycles, including that t the mode I crack propagation was influenced by the number of dry-wet cycles with the crucial parameters, fracture toughness, material parameters, cracking time and average crack propagation speed, and as the increase of dry-wet cycle number, the crack propagation speed increases, and the crack initiation time decreases. To understand the deterioration on the tensile strength of sandstone induced by wetting and drying cycles, Zhou et al. [15] proposed a decay model considering the effects of loading rate and cyclic wetting and drying deterioration based on, dynamic Brazilian. Feng et al. [16] investigate the dynamic mechanical properties and damage characteristics of lightweight foamed concrete under impact loading, considering the influence of strain rate and material density, concluding that the fractal dimension increases markedly with increasing strain rate, and the fractals present a transition behavior for different density materials. experimental study on the dynamic fracture mechanical properties of limestone after chemical corrosion, combining with the integrated method of nuclear magnetic resonance (NMR) system, a high-speed camera, the JR 3D scanning system, scanning electron microscope (SEM) and X-ray fluorescence (XRF) technology, concluding that a gradual increase in the fracture surface roughness due to the defects of the corrosion damage [17]. Weng et al. [18] studied the energy dissipation and dynamic fragmentation of dry and water saturated siltstones under sub-zero temperatures based on the comparison of dry and saturated siltstone specimens，indicating that the saturated specimens are more fragmented after the dynamic impact. Huang et al. [19] studied the stress-induced gradation evolution of granular materials under confined comminution. Li et al. [20] investigated the dynamic fracturing properties of marble after being subjected to multiple impact loadings, concluding that the larger the dynamic cumulative damage of the specimen is, the rougher the fracture surface, and the larger the area of the fracture surface. Energy is the internal factor of material failure, which runs through the whole process of material deformation and failure. The main way to study the failure mechanism of coal rock mass is to analyze the energy dissipation characteristics. Based on the principle of energy dissipation, scholars have carried out a series of experimental studies on the dynamic deformation and failure of different coal bodies. The energy dissipation [21], fractal feature [22] and energy storage property [23] of coal rock mass are analyzed, and the understanding of energy dissipation in the process of coal rock failure is improved.

According to the work aforementioned, the mechanical properties and fracture morphology of the rock and coal mass were intensively studied. The coal is an anisotropy medium consisting of pore-fracture system and matrix pores, as the water immersion, the friction and soluble minerals were disturbed, thereby the mechanical properties and the energy dissipation in failure process of the coal was changed. The failure type and its intensity evaluation index of coal subjected to different water contents and incident energy, and the corresponding in-site prevention methods are rarely studied. In this study, the mechanical properties and the energy dissipation in failure process of the coal with different water contents were tested, to study the water-effect on the prohibiting of coal bump in a complex geology. The SHPB system, combined with high-speed camera, and fractal dimension was employed, and the characteristic of stress-stain, stress peak and fracture evolution and morphology were analyzed. The crack propagation rule was clarified, and the dynamic failure mechanism of the water-soaked coal samples under the high loading rate was proposed.

2. EXPERIMENTAL SETUP

2.1. Coal sample preparation

The coal samples were collected from the panel of #401103 in Hujiahe Coal Mine located in Shanxi province. There were several serious coal bump in the mining process. The coal samples with proper integrity and homogeneity were selected and prepared with a dimension of Φ50mm × 25mm. The disc samples were ground and polished into non-parallelism less than 0.05 mm and diameter deviation of the end faces below 0.02 mm. A total of 75 samples were prepared and tested. The sample is prepared according to the standards of international society of rock mechanics, and the machining accuracy meets the requirements of dynamic mechanical test preparation [24].

The samples were divided into five groups with the number of 15, according to the water contents. The preparation procedures as follows:

(1) All samples were dried in a constant temperature drying oven to obtain dry coal samples (water content 0), the weight being m_{dry};

(2) Water-saturated coal samples were prepared by using the vacuum pumping device, according to the GB/T 23561-2009 standard. The weight of the water-saturated coal sample is m_{sat}. Thus the saturated water content is given by

$$w_{sat} = \frac{m_{sat} - m_{dry}}{m_{dry}} \times 100\% \tag{1}$$

(3) The coal samples were soaked in water according to the natural soaking method. The dry coal samples were placed into a water tank containing purified water. The samples were taken out every 30 min, and the water was wiped off from the surface. Then, the samples were weighed. When the weight of the coal samples approached the specified value for the saturated samples, the time interval for weight measurement was reduced until the specified value was reached. The weight of the saturated sample was m_{mea}. Subsequently, the coal samples were wrapped in polyethylene film to prevent further changes in the water content. The range of water content was determined according to [25]. The above steps were repeated until the coal sample approached the middle-saturated state. The water content is calculated:

$$w_{mea} = \frac{m_{mea} - m_{dry}}{m_{dry}} \times 100\% \tag{2}$$

The water contents are 0, 1.765%, 2.136%, 2.627%, 3.174%, respectively.

2.2. Experimental device and procedure

The SHPB test system used in the experiment is developed by Central South University with a heterogeneous punch head, as shown in Fig. 1 [26]. The compression bar diameter was 50 mm, length was 1500 mm. Both the compression bar and punch head were made of high-strength alloy steel, with a density of 7800 kg/m^3, elastic modulus 210 GPa, longitudinal wave velocity 5190 m/s, and the impact waveform was sinusoidal, the specific schematic of the SHPB was shown in Fig. 2. The data acquisition system was composed of the SDY2107A dynamic strain gauge, DL850E Scope Corder, and FASTCAM SA-Z high-speed camera. The frame rate of the camera is 100000 frames per second and the resolution is 256 × 384.

The initial impact test showed that the coal samples had a relatively small tensile strength. The impact pressure of initial test is 0.3MPa, and the dynamic tensile strength of coal sample is 3.26 MPa. The impact air pressures used for the tensile test were 0.30, 0.35, 0.40, 0.45, and 0.50 MPa, respectively. Three parallel samples were tested under each air pressure. Thus, the dynamic tensile tests were performed for a total of 75 times. During each test, Vaseline was first applied to the position where the compression bar met the coal samples. This was done so that the coal samples would be kept in close contact with the compression bar to

reduce friction [27]. The bullet speed and incident wave amplitude were controlled by adjusting the nitrogen pressure.

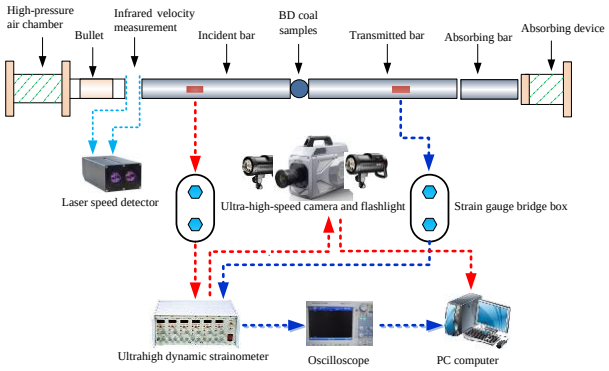

Fig. 1 – SHPB, ultra-high-speed camera system, and digital signal processing system.

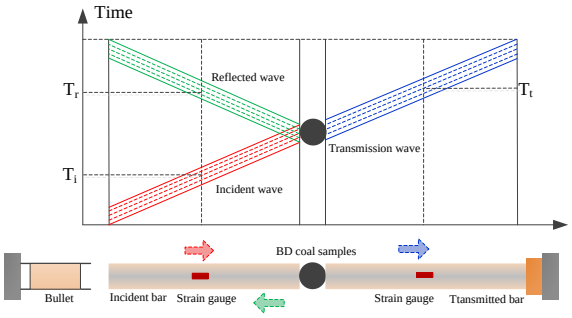

Fig. 2 – Schematic diagram of test principle.

3. RESULT AND ANALYSIS

3.1. Validation of the dynamic stress equilibrium

As shown in Fig. 3, the sum of the stress due to the incident and reflected waves was almost identical to that of the transmitted wave [26]. This finding indicated that during the Brazil disc splitting test, the coal samples reached dynamic stress equilibrium, and the dynamic tensile test was verified. All experimental results were subjected to strict stress equilibrium validation during data processing. The data that did not conform to the equilibrium were eliminated.

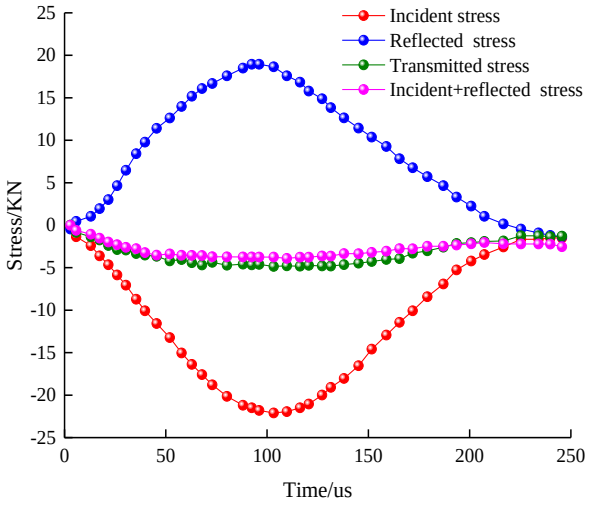

Fig. 3 – Validation of dynamic stress equilibrium in typical samples.

3.2. Energy dissipation characteristics

Under impact loading, the voltage signals on the incident bar and transmission bar are collected by the ultra dynamic strain gauge. Based on the one-dimensional stress wave theory, the electrical signal is converted into strain, and the three wave method is used to calculate the dynamic stress-strain relationship of coal sample under impact loading. The energy carried in the process of stress wave propagation in impact test can be calculated according to the following formula:

$$W_I = AEC_B \int \varepsilon_I{}^2(t)\,\mathrm{d}t \tag{3}$$

$$W_R = AEC_B \int \varepsilon_R{}^2(t)\,\mathrm{d}t \tag{4}$$

$$W_T = AEC_B \int \varepsilon_T{}^2(t)\,\mathrm{d}t \tag{5}$$

where $\varepsilon_I(t)$, $\varepsilon_R(t)$ and $\varepsilon_T(t)$ represent the incident strain, reflected strain and transmitted strain at time *t* respectively, W_l, W_R, W_T represent the energy carried by incident wave, reflected wave and transmitted wave respectively, *A*, *E*, C_B represent the cross-sectional area, elastic modulus and acoustic propagation velocity of elastic rod respectively.

Ignoring the energy loss caused by the friction between the elastic rod and the specimen in the process of stress wave propagation, the energy absorbed and dissipated by the specimen failure under impact is as follows:

$$W_S = W_I - W_R - W_T \tag{6}$$

In order to reduce the error caused by the size difference of impact specimen, the test results are treated as the dissipated energy per unit volume of specimen:

$$\varepsilon_s = \frac{W_S}{V} \tag{7}$$

$$\lambda = \frac{W_S}{W_I} \tag{8}$$

where: ε_s is the dissipative energy density of specimen failure, *V* is the volume of specimen, and λ is the proportion of dissipative energy.

The time energy curve of a typical dynamic tensile specimen is shown in Fig. 4. It can be seen from the figure that all kinds of energy increase with time under impact loading, and the change of energy growth is almost the same in the range of 0 ~ 30 us. After 30 us, the growth slope of absorption energy and transmission energy is roughly the same, the growth slope of reflection energy is the smallest, and the growth slope of incident energy is the largest. The energy change curve of coal sample is divided into three stages from the perspective of absorbed energy [28].

The I stage: 0 ~ 30 us, the coal sample is in the elastic deformation stage, and the absorbed energy is stored in the form of elastic property.

The II stage: 30 ~ 165 us, the absorption energy and transmission energy have the same growth rule, and the growth rate is greater than the reflection energy. Due to the mismatch of wave impedance between the elastic rod and the sample, the stress wave propagates repeatedly among the incident rod, the sample and the transmission rod, and all kinds of energy can be supplemented. Moreover, because the stress wave strength is greater than the ultimate tensile strength of the coal sample, the stress wave propagates back and forth to damage the coal sample, and the internal primary crack expands, and the absorbed energy continues to increase.

The III stage: 165 – 230 us, the slope of absorption energy growth gradually increases. In this stage, the primary cracks in coal samples expand rapidly, and a large number of new cracks are produced. The cracks gradually penetrate until the coal sample is damaged, and the energy value finally tends to a stable value.

According to formula (3)–(7), the energy of coal samples with different water content under impact load is calculated as shown in Table 1. When analyzing the energy distribution of tensile failure of coal samples, we often pay attention to the evolution characteristics of the proportion and density of dissipated energy, which respectively reflect the ability of the sample to absorb energy and the ability of the sample to use the absorbed energy for crushing work. Therefore, the following mainly analyzes the evolution laws of the proportion λ and dissipated energy density ε_s of coal samples with different water content.

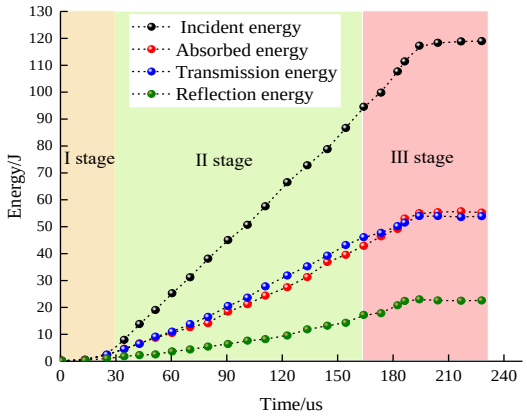

Fig 4 – Sample energy change curve.

Table 1

Statistical distribution of sample energy

Number	average moisture content /%	Loading pressure /MPa	Incident energy W_I/J	Absorbed energy W_S/J	Proportion of dissipated energy λ	Dissipative energy density ε_s/J·m^{-3}
BD-1-0.30	0	0.30	39.71	8.38	0.211	271.42
BD-1-0.35		0.35	56.94	12.19	0.214	246.90
BD-1-0.40		0.40	94.28	20.08	0.213	391.49
BD-1-0.45		0.45	113.66	23.53	0.207	457.88
BD-1-0.50		0.50	132.84	28.16	0.212	558.24
BD-2-0.30	1.765	0.30	41.24	9.86	0.239	197.57
BD-2-0.35		0.35	53.11	13.49	0.254	270.23
BD-2-0.40		0.40	96.35	23.99	0.249	482.42
BD-2-0.45		0.45	109.36	27.89	0.255	553.66
BD-2-0.50		0.50	136.31	34.49	0.253	666.30
BD-3-0.30	2.136	0.30	37.68	9.38	0.249	181.99
BD-3-0.35		0.35	60.84	15.64	0.257	312.54
BD-3-0.40		0.40	93.18	24.41	0.262	482.48
BD-3-0.45		0.45	111.26	28.71	0.258	578.14
BD-3-0.50		0.50	129.56	34.33	0.265	687.22
BD-4-0.30	2.627	0.30	39.98	11.23	0.281	225.45
BD-4-0.35		0.35	56.18	15.90	0.283	308.18
BD-4-0.40		0.40	92.58	26.20	0.283	506.02
BD-4-0.45		0.45	115.36	33.22	0.288	682.12
BD-4-0.50		0.50	131.87	38.77	0.294	802.35
BD-5-0.30	3.174	0.30	38.31	11.30	0.295	238.27
BD-5-0.35		0.35	54.53	16.90	0.310	328.99
BD-5-0.40		0.40	92.05	28.81	0.313	577.50
BD-5-0.45		0.45	115.25	35.50	0.308	737.58
BD-5-0.50		0.50	135.86	42.25	0.311	858.45

Note: The data in the table are the mean values of each group of parallel tests.

As shown in Fig. 5, the proportion of dissipated energy of coal samples with different water content is stable with the increase of impact load, but under the same impact pressure, the water content affects the propagation velocity of stress wave in coal samples. In other words, saturated coal samples have higher wave impedance, and the more the wave impedance is, the more the dissipated energy of stress wave will be, therefore, the proportion of dissipated energy increases with water content of coal samples under the same loading pressure. As shown in Fig. 6, the dissipation energy density of different water-bearing coal samples increases linearly with the impact load, which is similar to the results of Gu et al. [33]. Meanwhile, the increase rate of dissipated energy density value of saturated coal sample is greater than that of other state coal samples, and the dry coal sample is the smallest. When the incident energy is small, the dissipated energy density value of coal sample has little difference.

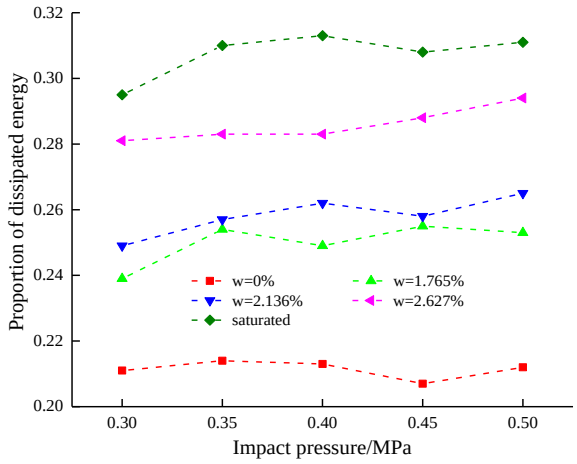

Fig. 5 – The proportion of dissipated energy of different water-bearing coal samples.

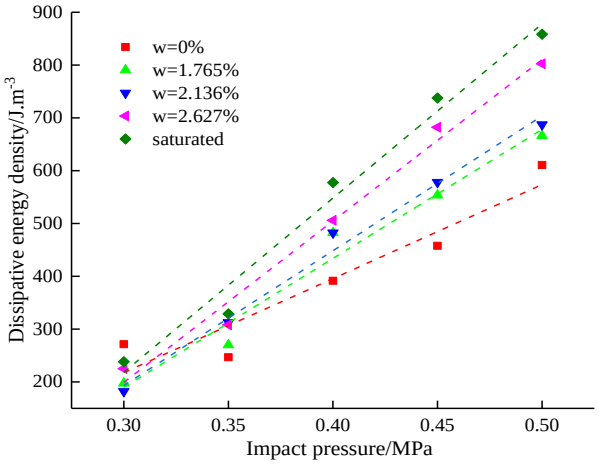

Fig. 6 – Dissipated energy density of different water-bearing coal samples.

It was found that the proportion of dissipated energy and the density of dissipated energy are affected by water content. The proportion and density of dissipated energy of dry coal sample are the smallest, and that of saturated coal sample is the largest. After the coal sample is saturated with water, the primary fracture channel is filled, the sample tends to be more "uniform structure", the overall stress concentration phenomenon under impact load is weakened, and more energy is consumed for sample damage and fracture. When the incident energy of the stress wave is small, the coal sample is in the elastic deformation stage. With the increase of the incident energy, the coal sample is in the plastic stage. At this time, the primary cracks expand and produce a large number of new cracks, weakening the transmission wave propagation. If the incident energy is large, the coal sample is broken into powder instantly, the stress wave propagation is terminated, and the energy value of the coal sample tends to a stable maximum.

4. THE FRACTAL CHARACTERISTICS

The fragmentation degree of coal and rock mass can be characterized by the fractal dimension, the larger fragmentation corresponding to the higher value of fractal and small pieces volume [30]. Considering the water-effect on the strength of coal and rock mass, the relationship of water content and fragmental degree can be characterized by the fractal characteristics.

The fractal dimension can be calculated using debris mass-equivalent edge length [31], the expression was shown below:

$$D = 3 - \alpha \tag{9}$$

$$\alpha = \frac{\lg\left(M_{Leq} / M\right)}{\lg L_{eq}} \tag{10}$$

where, M_{Leq} represents the pieces mass corresponding to the equivalent length of L_{eq}, D is the fractal dimension, α is the slope value of $\frac{M_{Leq}}{M - L_{eq}}$ in the two-pair coordinate, M_{Leq} / M is the percentage content for the equivalent length below the L_{eq}. The coal species sieve weighting device is shown in Fig. 9.

(a) (b)

Fig. 9 – Screening weighing device for coal sample debris: a) standard sieve, b) electronic scale.

As seen in Fig. 10, the trends of the curves are mixed, some with increasing/decreasing slopes and some with decreasing slopes (rates). Please rephrase the comment. Compared with the dry coal, the fractal dimensionality of saturated coal is the largest under impact of the same shock pressure. The damage pattern of the sample is shown in Fig. 11, the dry coal sample split in two halves for the shock pressure of 0.30 MPa, combined with small amount of debris. In contrast, the saturated coal sample broken into chunks, accompanied by a large amount of debris. For the shock pressure of 0.5 MPa, dry coal samples are broken into small pieces and saturated coal samples are broken into powders. The deformation damage of the sample is accompanied by the dissipation of energy, the greater the impact pressure, the greater the energy absorbed by the coal sample, resulting in the greater degree of crushing [32].

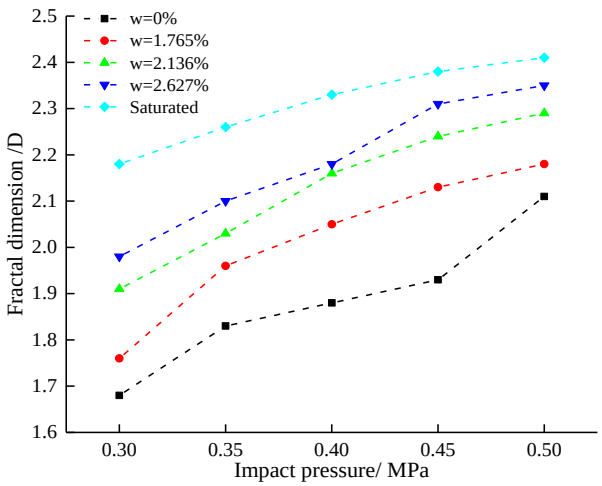

Fig. 10 – Relationship between fractal dimension of different water bearing coal samples and impact pressure.

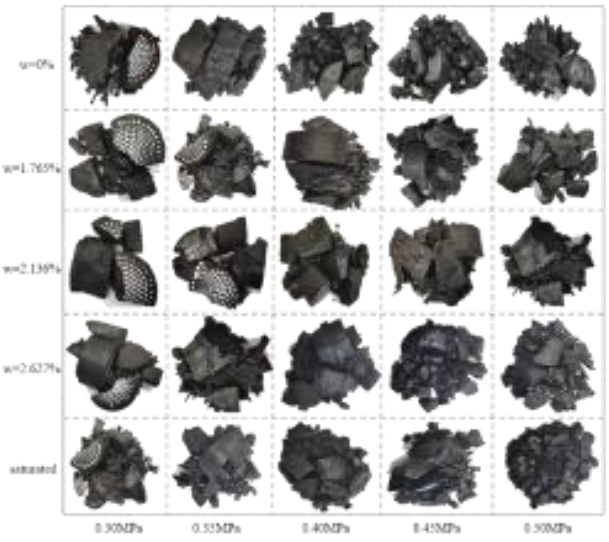

Fig. 11 – Failure mode of specimens.

5. CONCLUSION

(1) The dissipative energy density of coal samples with different water content increases linearly with the increase of impact load. The increasing rate of dissipative energy density of saturated coal samples is higher than that of coal samples in other states. When the incident energy is small, the difference of dissipative energy density of coal samples is not significant.

(2) Under the impact load, the dry coal sample is prone to stress concentration at the end of the primary fracture, resulting in damage, while the primary fracture channel of the saturated coal sample is filled, the sample tends to be more "uniform structure", the overall stress concentration phenomenon is weakened, and more energy is consumed for damage.

(3) The failure morphology is characterized by the tensile splitting in coal samples. The cracks developed along the loading direction after being initiated along the incident direction under the impact load. The growth of fracture surface consisting of microcracks development, convergent, and penetration. As the water content increased, the crack morphology was more complex, and the fragmentation was more severe.

(4) For lower rate of impact loading, water presented a weakening effect on the strength of the coal. In contrast, the inertia effect of coal hinders the initiation and propagation of cracks, resulting in an increase in dynamic tensile strength at a higher impact load rate. hindered crack initiation and propagation, resulting in the increase of the dynamic tensile strength under the higher rate of impact loading. The dynamic mechanical properties of the water-saturated coal samples are dominated by the weakening and strengthening effects cause by the impact pressure and water content.

ACKNOWLEDGEMENTS

This work was supported by the National Natural Science Foundation of China (no.51634007), the Hefei Comprehensive National Science Center Energy Research Institute (Anhui Energy Laboratory) project (21KZS217). Research on basic theory and key technology of deep coal green safety intelligent precision mining (no.GXXT-2019-029).

REFERENCES

1. L. CHEN, E. WANG, J. OU, J. FU, *Coal and gas outburst hazards and factors of the No. B-1 Coalbed, Henan, China*, Geosciences Journal, **22**, *1*, pp. 171–182, 2018.
2. H. TU, S. TU, Y. YUAN, F. WANG, Q. BAI, *Present situation of fully mechanized mining technology for steeply inclined coal seams in China*, Arabian Journal of Geosciences, **8**, p. 4485–4494, 2015.
3. H. WANG, Y. CHENG, L. YUAN. *Gas outburst disasters and the mining technology of key protective seam in coal seam group in the Huainan coalfield*, Natural Hazards, **67**, pp. 763–782, 2013.
4. A.D. BARR, S.D. CLARKE, M. PETKOVSKI, A. TYAS, S.E. RIGBY, J. WARREN, S. KERR, *Effects of strain rate and moisture content on the behaviour of sand under one-dimensional compression*, Experimental Mechanics, **56**, *9*, pp. 1–15, 2016.
5. S. RENLIANG, S. YONGWEI, S. LIWEI, B. YAO, *Dynamic property tests of frozen red sandstone using a split hopkinson pressure bar*, Earthquake Engineering and Engineering Vibration, **18**, *3*, pp. 511–519, 2019.
6. H. LUO, W.L. COOPER, H. LU, *Effects of particle size and moisture on the compressive behavior of dense Eglin sand under confinement at high strain rates*, International Journal of Impact Engineering, **65**, *3*, pp. 40–55, 2014.
7. L. VARLEY, M.E. RUTHERFORD, L. ZHANG, A. PELLEGRINO, *The mechanical response of wet volcanic sand to impact loading, effects of water content and initial compaction*, Journal of Dynamic Behavior of Materials, **6**, *3*, pp. 358–372, 2020.
8. C.J. LI, Y. XU, Y.T. ZHANG, *Study on energy evolution and fractal characteristics of fractured coal rock association under impact load*, Journal of rock mechanics and engineering, **38**, pp. 2231–2241, 2019.
9. Y. DENG, M. CHEN, Y. JIN, D. ZOU, *Theoretical analysis and experimental research on the energy dissipation of rock crushing based on fractal theory*, Journal of Natural Gas Science and Engineering, **33**, pp, 231–239, 2016.
10. D. AI, Y. ZHAO, Q. WANG, C. LI, *Crack propagation and dynamic properties of coal under SHPB impact loading: Experimental investigation and numerical simulation*, Theoretical and Applied Fracture Mechanics, **105**, art. 102393, 2020.
11. D. AI, Y. ZHAO, Q. WANG, C. LI, *Experimental and numerical investigation of crack propagation and dynamic properties of rock in SHPB indirect tension test*, International Journal of Impact Engineering, **126**, pp. 135–146, 2019.

12. Z. ZHOU, X. CAI, D. MA, L. CHEN, S. WANG, L. TAN, *Dynamic tensile properties of sandstone subjected to wetting and drying cycles*, Construction and Building Materials, **114**, pp. 46–61, 2018.
13. S. CAO, G. XUE, W. SONG, Q. TENG, *Strain rate effect on dynamic mechanical properties and microstructure of cemented tailings composites*, Construction and Building Materials, **247**, art. 118537, 2020.
14. Y. ZHAO, S. LIU, Y. JIANG, K. WANG, Y. HUANG, *Dynamic tensile strength of coal under dry and saturated conditions*, Rock Mechanics and Rock Engineering, **49**, pp. 1709–1720, 2016.
15. Z.L. ZHOU, J. ZHOU, Y. ZHAO, L.J. CHEN, C.J. LI, *Microscopic failure mechanism analysis of rock under dynamic brazilian test based on acoustic emission and moment tensor simulation*, Frontiers in Physics, **8**, art. 592483, 2021.
16. S. FENG, Y. ZHOU, Y. WANG, M. LEI, *Experimental research on the dynamic mechanical properties and damage characteristics of lightweight foamed concrete under impact loading*, International Journal of Impact Engineering, **140**, art. 103558, 2020.
17. L. YU, Z. ZHANG, J. WU, R. LIU, H. QIN, P. FAN, *Experimental study on the dynamic fracture mechanical properties of limestone after chemical corrosion*, Theoretical and Applied Fracture Mechanics, **108**, art. 102620, 2020.
18. L. WENG, Z. WU, Q. LIU, Z. WANG, *Energy dissipation and dynamic fragmentation of dry and water-saturated siltstones under sub-zero temperatures*, Engineering Fracture Mechanics, **220**, art. 106659, 2019.
19. J.Y. HUANG, S.S. HU, S.L. XU, S.N. LUO, *Fractal crushing of granular materials under confined compression at different strain rates*, International Journal of Impact Engineering, **106**, pp. 259–265, 2017.
20. D.Y. LI, Z.Y. HAN, X.L. SUN, T. ZHOU, X.B. LI, *Dynamic mechanical properties and fracturing behavior of marble specimens containing single and double flaws in SHPB tests*, Rock Mechanics and Rock Engineering, **52**, pp. 1623–1643, 2018.
21. H. WU, B. DAI, L. CHENG, R. LU, G.Y. ZHAO, W.Z. LIANG, *Experimental study of dynamic mechanical response and energy dissipation of rock having a circular opening under impact loading*, Mining, Metallurgy & Exploration, **38**, *2*, pp. 1111–1124, 2021.
22. M. JU, Jianchun LI, Jing LI, J. ZHAO, *Loading rate effects on anisotropy and crack propagation of weak bedding plane-rich rocks*, Engineering Fracture Mechanics, **230**, art. 106983, 2020.
23. L. YU, A. FU, Q. YIN, H. JING, T. ZHANG, H. QIN, *Dynamic fracturing properties of marble after being subjected to multiple impact loadings*, Engineering Fracture Mechanics, **230**, art. 106988, 2020.
24. Y.X. ZHOU, K. XIA, X.B. LI, H.B. LI, G.W. MA, J. ZHAO, Z.L. ZHOU, F. DAI, *Suggested methods for determining the dynamic strength parameters and mode-I fracture toughness of rock materials*, International Journal of Rock Mechanics and Mining Sciences, **49**, pp. 105–112, 2011.
25. Z. PAN, L.D. CONNELL M. CAMILLERI, L. CONNELLY, *Effects of matrix moisture on gas diffusion and flow in coal*, Fuel, **89**, *11*, pp. 3207–3217, 2010.
26. Z. WEI, K. YANG, X.L. CHI, X. HE, X.Y. ZHAO, J.Q. ZHANG, *Dynamic tensile properties deformation and failure testing of impact-loaded coal samples with various water content*, Scientific Reports, **11**, *1*, art. 7096, 2021.
27. S. LI, G. NI, H. WANG, M. XUN, Y. XU, *Effects of acid solution of different components on the pore structure and mechanical properties of coal*, Advanced Powder Technology, **31**, *4*, pp. 1736–1747, 2020.
28. J. FENG, E. WANG, Q. HUANG, H. DING, X. ZHANG, *Experimental and numerical study of failure behavior and mechanism of coal under dynamic compressive loads*, International Journal of Mining Science and Technology, **30**, pp. 613–621, 2020.
29. Z. ZHOU, X. CAI, W. CAO, X. LI, C. XIONG, *Influence of water content on mechanical properties of rock in both saturation and drying processes*, Rock Mechanics and Rock Engineering, **49**, *8*, pp. 3009–3025, 2016.
30. Z.X. ZHANG, S.Q. KOU, J. YU, Y. YU, L.G. JIANG, P-A. LINDQVIST, *Effects of loading rate on rock fracture*, International Journal of Rock Mechanics and Mining Sciences, **36**, *5*, pp. 597–611, 1999.
31. M.C. HE, G. YANG, J. MIAO, X. JIA, T. JIANG, *Classification and research methods of rock burst experiment debris*. Journal of rock mechanics and engineering, **28**, pp. 1521–1529, 2009.
32. Y. CHEN, H. WU, H. PU, K. ZHANG, F. JU, Y. WU, J. LIU, *Investigations of damage characteristics in rock material subjected to the joint effect of cyclic loading and impact*, Energies, **13**, art. 2154, 2020.
33. H. GU, M. TAO, X. LI, W. CAO, Q. LI, *Dynamic tests and mechanical model for water-saturated soft coal with various particle gradations*, International Journal of Rock Mechanics and Mining Sciences, **132**, art. 104386, 2020.

Received January 16, 2022